

ORIGINAL RESEARCH

Open Access



Near real-time indicators of burn severity in the western U.S. from active fire tracking

Elijah Orland^{1,2*}, Tempest D. McCabe^{1,3}, Yang Chen⁴, Rebecca C. Scholten⁴, Zeb Becker^{1,3}, Rachel A. Loehman⁵, James T. Randerson⁴, Shane R. Coffield^{1,3}, Tianjia Liu⁶, Alexey N. Shiklomanov¹, Kurtis Nelson⁷, Birgit Peterson⁷, Melanie B. Follette-Cook¹ and Douglas C. Morton¹

Abstract

Background Timely information on wildfire burn severity is critical to assess and mitigate potential post-fire impacts on soils, vegetation, and hillslope stability. Tracking individual fire spread and intensity using satellite active fire data provides a pathway to near real-time (NRT) information. Here, we generated a large database (n = 2177) of wildfire events in the western United States (U.S.) between 2012 and 2021 using active fire detections from the Visible Infrared Imaging Radiometer Suite (VIIRS) sensor on the Suomi National Polar-orbiting Partnership (SNPP) satellite and the Fire Events Data Suite (FEDS) algorithm to track large fire growth every 12 h. We integrated fire tracking data with final fire perimeters and burn severity data from the Monitoring Trends in Burn Severity (MTBS) program to evaluate the relationship between burn severity and fire behavior metrics derived from the fire tracking approach, including the rate of fire spread and average fire radiative power (FRP) of fire detections for each 12-h growth increment.

Results When stratified by vegetation type, FRP and rate of spread metrics were positively correlated with classified burn severity for each 12-h growth increment, highlighting the potential to rapidly identify areas of high and low severity burning. In forests, integrated measures of FRP over the fire lifetime captured persistent flaming and smoldering that compensated for initial differences between AM (01:30) and PM (13:30) fire detections. Predictive modeling of these relationships based on multiple fire behavior indicators and vegetation type from the LANDFIRE program yielded an accuracy of 78% for the separation of unburned/low and moderate/high burn severity classes.

Conclusions These results demonstrate the ability to capture within-fire differences in burn severity using NRT indicators from fire tracking to assist with emergency management and disaster preparedness for post-fire hazards, such as landslides, debris flows, or changes in stream flow and water quality. As VIIRS data are available within minutes of each satellite overpass in the U.S., rapid estimates of burn severity based on fire tracking can be made days or weeks before a large wildfire is fully contained.

Keywords Remote sensing, Post fire, Machine learning, Burn severity, Fire tracking, Fire intensity

Resumen

Antecedentes La información oportuna sobre la severidad de los incendios es crítica para determinar y mitigar los potenciales impactos post-fuego sobre los suelos, la vegetación, y la estabilidad de las laderas de montaña. El seguimiento de la velocidad de propagación de cada incendio activo usando datos de satélites, provee de una vía rápida para obtener información en tiempo real (NRT). En este trabajo, generamos una gran base de datos de

*Correspondence: Elijah Orland elijah.orland@nasa.gov; eliorland@att.net Full list of author information is available at the end of the article



Orland et al. Fire Ecology (2025) 21:55 Page 2 of 18

eventos de incendios (n = 2.177) en el oeste de los EEUU entre 2012 y 2021, usando detecciones activas del sensor de imágenes radiométricas infrarrojas (VIIRS) del satélite *Suomi National Polar-Orbiting Partnership* (SNPP), y de un algoritmo de un conjunto de datos de eventos de incendios (FEDS). Esto permite, cada 12 horas, rastrear el crecimiento de grandes incendios. Integramos los datos de rastreo de estos incendios con los perímetros finales del fuego y con las detecciones cada 12 horas sobre la severidad de estos incendios basados en el programa de monitoreo de las tendencias en severidad de las quemas (MTBS), para evaluar la relación entre la severidad de los incendios y las métricas de comportamiento del fuego derivadas de la aproximación del rastreo, incluyendo la tasa de propagación del fuego, y el promedio del poder radiante del fuego (FRP) de las detecciones para cada 12 h de incremento en el crecimiento del fuego.

Resultados Cuando fueron estratificados por tipo de vegetación, el FRP y las métricas de propagación fueron positivamente correlacionadas con la clasificación de la severidad del fuego cada 12 h de incremento en el crecimiento del incendio, subrayando el potencial para identificar rápidamente áreas de alta y baja severidad del fuego. En bosques, las medidas integradas de FRP sobre la duración del incendio capturaron llamas y material en combustión de manera permanente, que compensaron las diferencias iniciales de detección entre la 01:30 AM y las 13:30 PM. El modelo predictivo de esas relaciones basadas en indicadores múltiples de comportamiento del fuego y tipos de vegetación del programa LANDFIRE, tuvieron una exactitud del 78% para la separación de clases de severidad de "no quemado/baja", y "moderado/alta intensidad".

Conclusiones Estos resultados muestran la habilidad para capturar las diferencias de severidad entre fuegos usando indicadores del rastreo de NRT y poder asistir con el manejo de la emergencia y la preparación del desastre y los peligros del post fuego como los deslizamientos de laderas, el flujo de residuos, o cambios en el flujo de las corrientes de los arroyos y la calidad del agua. Dado que los datos de VIIRS están disponibles dentro de pocos minutos luego de que el satélite haya sobrevolado los EEUU, las estimaciones rápidas de la severidad basadas en el rastreo del fuego puede hacerse muchos días o semanas antes de que un gran incendio sea totalmente contenido.

Background

Wildfires have substantial and interconnected impacts on vegetation, soils, and hydrology (Bowman et al. 2009) that vary as a function of burn extent and intensity (e.g., Adams 2013; Coop et al. 2019; Schwilk & Ackerly 2001). Fuel consumption and fire-induced vegetation mortality alter biogeochemical cycles and contribute to greenhouse gas emissions (e.g., Crutzen & Andreae 1990; Hao & Liu 1994; Kasischke et al. 1995; Seiler & Crutzen 1980; Van Der Werf et al. 2003, 2017). Post-fire changes in vegetation structure and composition also change surface albedo (Randerson et al. 2006), reduce the infiltration capacity of burned soils (Debano 2000; Letey 2001), trigger soil nutrient and chemical losses (Alexakis et al. 2021; Chen et al. 2010; Neff et al. 2005; Rovira et al. 2012), and increase the available sediment for mobilization downslope (Florsheim et al. 1991, 2016; Gabet 2003; Lamb et al. 2011, 2013). Combined, these impacts lead to longitudinal changes to the hydrologic cycle, including reductions in evapotranspiration (Ahmad et al. 2024; Bond-Lamberty et al. 2009; Kang et al. 2006; Roche et al. 2018) an increase in overland flow (Scott et al. 1998; Vega & Díaz-Fierros Viqueira 1987; Wells 1981) and greater risk of catastrophic debris flows (Cannon 2001; Cannon & DeGraff 2009; Kean et al. 2011; Lancaster et al. 2021). As wildfires in the western United States and other fire-prone regions become more frequent and intense (Abatzoglou & Williams 2016; Cunningham et al. 2024; Mueller et al. 2020; Westerling et al. 2006), the expedited delivery of burn severity data is crucial for assessing fire effects and for allocating resources to manage post-fire hazards.

One common approach to assess burn severity relies on pre-fire and post-fire satellite imagery to estimate the differenced or "delta" normalized burn ratio (dNBR)-a metric sensitive to the loss of live vegetation cover and soil exposure following burning (Eidenshink et al. 2007; Key & Benson 2006). As such, mapped dNBR within a burn scar based on Landsat or Sentinel-2 imagery is a common input for classifying burn severity, as used in standard products from the Monitoring Trends in Burn Severity (MTBS) or Burned Area Emergency Response (BAER) programs. These same image sources can also be used to derive alternative indices such as the Relativized dNBR (RdNBR) (Miller & Thode 2007) or the Relativized Burn Ratio (RBR) (Parks et al. 2014). Remote sensing-based metrics of burn severity vary in their ability to accurately represent field conditions, as index suitability changes based on fuel type and intended use case (Epting et al. 2005; Miller & Thode 2007; Morgan et al. 2014; Parks et al. 2014; Picotte & Robertson 2011; Whitman et al. 2018).

One of the key limitations of using remote sensingbased indices for assessing burn severity is the need Orland et al. Fire Ecology (2025) 21:55 Page 3 of 18

for post-fire imagery, given that image acquisition during or immediately following a wildfire may be delayed by clouds, smoke, or satellite revisit time. This time gap between the burn date and assessment date introduces uncertainty in the estimate of burn severity and delays the use of these data for situational awareness in response to a fire event. For groups tasked with emergency response—such as BAER teams in the United States—uncertainties tied to the availability of cloud-free imagery represent a barrier for responsive planning and management based on delays in mapping efforts to identify areas of elevated risk requiring immediate assessment and/or treatment. Additionally, longitudinal fire impacts such as delayed tree mortality may only become visible during the following growing season; for capturing these effects, "extended" MTBS assessments traditionally rely on imagery acquired 1 year after the fire to provide a more thorough picture of vegetation response (Key & Benson 2006; Eidenshink et al. 2007). Given these limitations, there is an opportunity to develop near real-time (NRT) approaches that draw on complementary satellite information to assist with burn severity assessments during and immediately following a large fire event prior to the availability of standard MTBS and BAER products.

One pathway for anticipating estimates of burn severity is to leverage pre-fire information. For example, using a combination of airborne light detection and ranging (lidar) and satellite-based land surface albedo measurements, Fernández-Guisuraga et al. (2021) examined the link between pre-fire vegetation structure and burn severity, highlighting the correlations between canopy height and volume with Composite Burn Index (CBI) and dNBR values. Similarly, Staley et al. (2018) linked historical distributions of dNBR values with existing vegetation type (EVT) classifications derived from LANDFIRE products (Rollins 2009). Using machine learning or related methods, many data-driven studies also demonstrate the important control of elevation on burn severity (Dillon et al. 2011; Estes et al. 2017; Holden et al. 2009; Wu et al. 2013). Finally, fire spread simulations (e.g., Finney 2006; Finney et al. 2011; Linn et al. 2002, 2020; Mell et al. 2007) have also been used to model fire behavior and serve as "scenario-based" assessments prior to burning. To date, these approaches have not incorporated active fire information made available in NRT to account for diurnal or day-to-day variability in fire behavior or intensity.

Satellite active fire detections provide information on the location and intensity of fire activity, and data are typically available within minutes to hours after each satellite overpass. For example, the Moderate Resolution Imaging Spectroradiometer (MODIS) sensors on NASA's Terra and Aqua satellites have already provided over 20 years of active fire detections at 1-km resolution (Giglio et al. 2016) and daily burned area estimates at 500-m resolution (Giglio 2018). The wealth of MODIS active fire and burned area data has spurred a range of approaches to delineate individual fire events, both on regional and global scales (Andela et al. 2019; Archibald & Roy 2009; Balch et al. 2013, 2020; Hantson et al. 2015; Lizundia-Loiola et al. 2020; Loboda & Csiszar 2007; Scaduto et al. 2020; Veraverbeke et al. 2014). However, many of these products rely on datasets not available in NRT, and thus are most appropriately used for retrospective analysis. Improvements in spatial resolution, sensitivity, and geolocation accuracy of active fire detections from the Visible Infrared Imaging Radiometer Suite (VIIRS) sensors (Schroeder et al. 2014) support new approaches to track individual fire events every 12 h (Andela et al. 2022; Chen et al. 2022). Recent work by Chen et al. (2022) introduced the Fire Events Data Suite (FEDS), an approach to use NRT active fire observations from the Suomi-NPP VIIRS sensor to iteratively track and reconstruct fire progression in 12-h intervals for the state of California from 2012 to 2020. The resulting FEDS data provide unprecedented insight into the variability in fire spread rate and intensity of large wildfires, thus promoting a framework to explore the relationships between fire behavior and burn severity.

In this study, we applied the FEDS algorithm to create a dataset of individual fire events for the Western U.S. from 2012 to 2021, aiming to systematically investigate the relationship between active fire characteristics and burn severity. We evaluated the potential for using multiple metrics of fire behavior derived in NRT from FEDS, exploring the tradeoffs between accuracy and latency for rapid assessments of burn severity. As wildfires in the U.S. can burn for weeks or months, these NRT indicators may fill an unmet need by providing timely updates on burn severity. Such information is crucial for situational awareness and responsive action both during and immediately after wildfire events.

Methods

Fire tracking

We used the FEDS algorithm (Chen et al. 2022) to generate 12-hourly fire progression data for the western U.S. from 2012 to 2021. The FEDS algorithm uses VIIRS 375-m active fire detections (Schroeder et al. 2014) to track individual fire progression at 12-h intervals that correspond to the cadence of VIIRS overpasses for a given area, with daily overpasses occurring at approximately 01:30 and 13:30 local time. Active fires are detected as thermal anomalies by the VIIRS sensor, where each 375-m active fire pixel indicates likely flaming or smoldering fire activity. Theoretical detection limits for sub-pixel burning in the VIIRS 375-m data product

Orland et al. Fire Ecology (2025) 21:55 Page 4 of 18

are reported to be as fine as 5-m², with this threshold varying as a function of day/night thermal contrast between fires and background conditions at the time of overpass, as well as the level of smoke or cloud obscuration (Schroeder et al. 2014). VIIRS active fire detection data contain supplementary information such as confidence flags, infrared brightness temperatures, and estimated fire radiative power (FRP) in megawatts (MW), representing the rate of energy output for that pixel at the time of observation. FRP can be directly linked to the rate of biomass combustion (Wooster et al. 2005) and therefore is used as a snapshot indicator of fire intensity and emissions at the time of satellite overpass.

To reconstruct the progression of historical fires, we used archived 375-m VNP14IMGML active fire location data to track the progression of all fires in the western U.S. from 2012 to 2021. The resulting dataset provides temporally consistent observations of fire spread in discrete 12-h periods across the study domain. Additionally, FEDS data capture multiple properties relevant to tracking active fire behavior, such as FRP, fire spread rate, and fire line length. As the FEDS algorithm was developed with a focus on tracking wildfires in California (Chen et al. 2022), the algorithm's application to the larger domain of the western U.S. in this study included minor improvements in the efficiency of the underlying clustering and merging components of the workflow to meet the increased computational demand. Additionally, fire tracking for the western U.S. region used projected coordinate systems (e.g., the US National Atlas Equal Area system, EPSG:9311) in contrast to the World Geodetic System (WGS) 84 geographic coordinate system (EPSG: 4326) used in Chen et al. (2022). See Data Availability for more information on data and code access. Because the FEDS algorithm relies on the preprocessed VIIRS-based data products outlined in Schroeder et al. (2014) and Schroeder & Giglio (2016), the same limitations discussed therein apply. This includes the possibility of false positive detections from static source hot spots and false negatives due to cloud or smoke cover.

In this analysis, we included all FEDS fire objects that intersected MTBS perimeters designated as wildfires with matching ignition dates within 10 days. Because MTBS includes all fires > 1000 acres in the western U.S., smaller fires in the FEDS database were excluded from this study. We computed the intersection-over-union (IOU) for all matches to allow additional filtering based on a quantitative representation of their spatial agreement. In total, the final dataset contains 2177 matched wildfires in the western U.S. between 2012 and 2021, representing a total fire-affected area of over 166,722 km² as mapped by the FEDS algorithm (Fig. 1).

Calculation of fire spread rate, intensity, and persistence

We analyzed fire spread based on the individual "increments" of fire growth during each 12-h interval (Fig. 2). Individual increments of fire growth were delineated by taking the geometric difference between fire perimeters derived at time t and those derived 12 h later. Each individual area of fire growth was assigned a unique index such that multiple segments of fire spread (each with different directions and locations on the fire perimeter) during the same 12-h period were tracked separately. We refer to these areas as "spread increments" or "growth increments," whose rate of growth can be expressed in units of km²/12-h. Each increment is categorized based on the timing of initial detection: increments marked as "PM" were constructed using active fire detections first observed at 13:30 local time. These increments include instantaneous measures of PM fire behavior (e.g., FRP) but nonetheless represent morning fire growth between 01:30 (the preceding overpass) and 13:30 (the current overpass) (Fig. 2). Similarly, growth increments linked to the AM overpass (01:30) mark afternoon fire growth.

To record information on fire intensity, we performed a spatial join between all spread increments and all VIIRS detections recorded for that fire. Notably, we recorded all pixels detected within each spread increment, including fire detections from the initial period of fire spread and any persistent burning detected within each increment over the lifetime of the fire. This approach provided multiple metrics of fire intensity and fire persistence (duration). For each increment of growth, we calculated the mean, maximum, and area normalized total FRP. Fire persistence was estimated using two metrics: (1) the number of unique 12-h periods with one or more VIIRS active fire detections within a given spread increment; and (2) the time difference between the first and last active fire detections, measured in hours.

For comparison with MTBS burn severity data, we performed zonal statistics between individual spread increments and classified MTBS pixels, recording the median MTBS pixel class within each polygon. MTBS severity classes in this analysis range from low/unburned (1), low (2), moderate (3), and high (4) severity; classes not pertaining to these groups, such as those representing enhanced regrowth (5) or no data (0), were excluded. Comparisons with MTBS data included both initial assessments focused on immediate fire impacts in low biomass systems, such as grasslands or small shrublands, as well as extended assessments using remote sensing imagery 1 year after the fire to capture delayed ecosystem effects in high biomass environments like dense shrublands or forests (Key & Benson 2006; Eidenshink et al. 2007). We analyzed the combined dataset using both assessment types and separately evaluated the Orland *et al. Fire Ecology* (2025) 21:55 Page 5 of 18

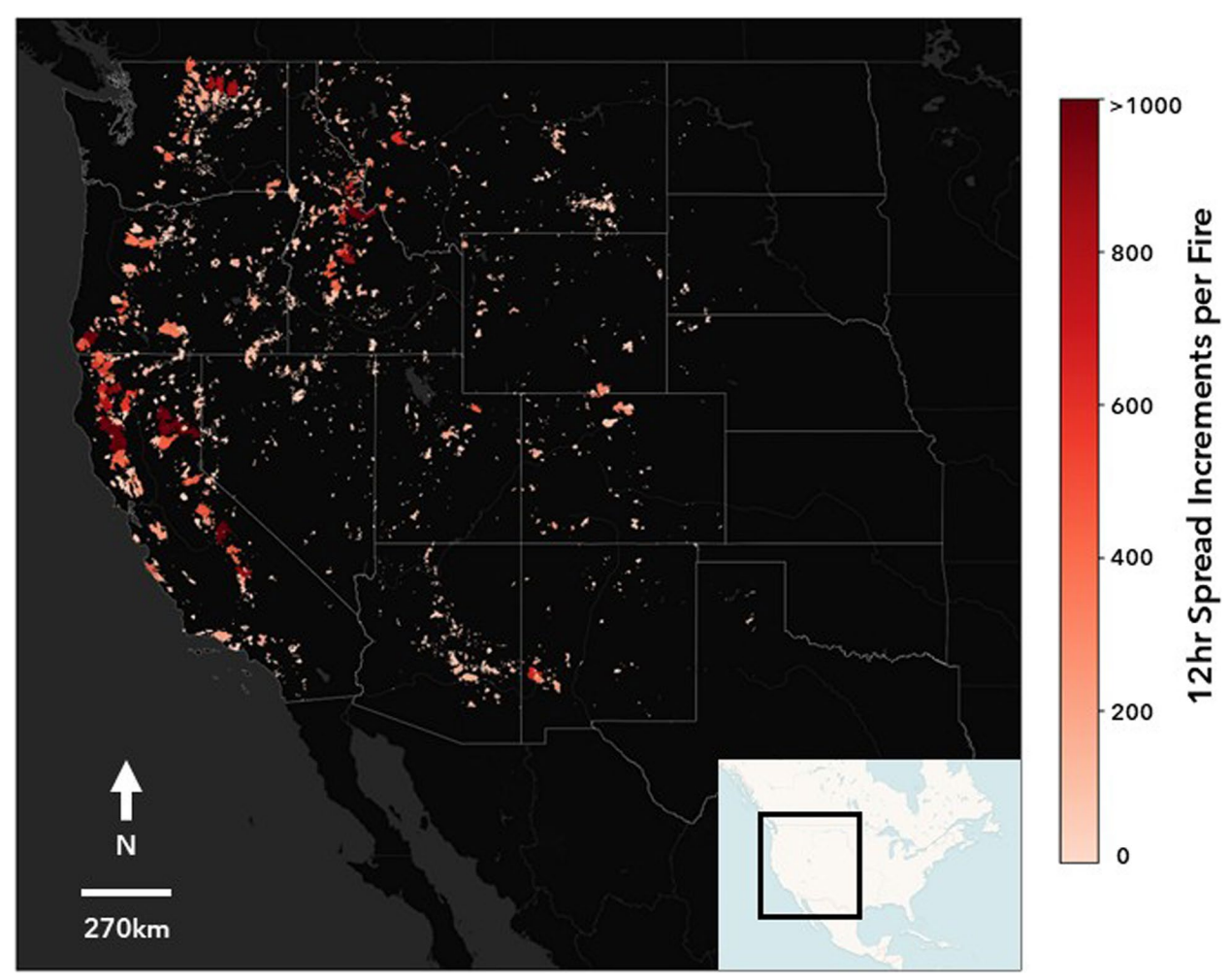


Fig. 1 Western U.S. wildfires from 2012 to 2021 included in the analysis (n = 2177), colored by the number of 12 h spread increments in each fire (total n = 56,700)

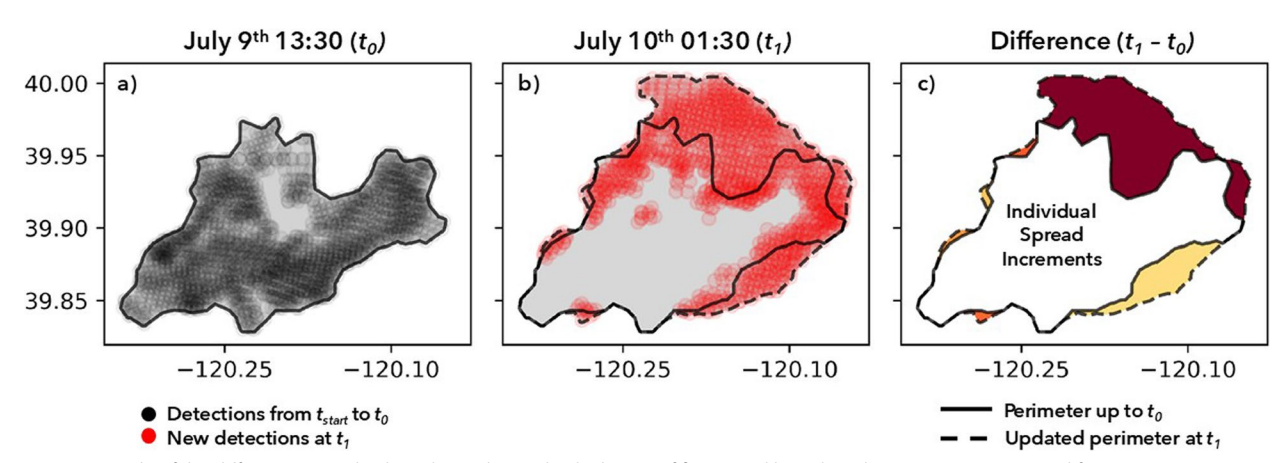


Fig. 2 Example of the differencing method used to isolate individual areas of fire spread based on the 2021 Sugar Fire in California. **a** FEDS perimeter on the afternoon of July 9th, 2021 (13:30). **b** The FEDS perimeter 12 h later at 01:30. **c** The geometric difference between these two perimeters highlighting areas of fire spread in that 12 h period, referred to in this work as fire growth or spread increments. Red shading in panel **b** denotes active fire detections during the 01:30 overpass, and areas of individual fire spread represent all growth that occurred between t₀ and t₁

Orland et al. Fire Ecology (2025) 21:55 Page 6 of 18

influence of initial versus extended assessment data on the relationships between fire behavior and burn severity. We used the LANDFIRE data products (Rollins 2009) matched to the appropriate fire year to estimate the most common existing vegetation type (EVT) prior to each fire to stratify the analysis of fire behavior and burn severity by vegetation type.

Finally, to ensure proper agreement between FEDS and MTBS products, we computed the overlap between each 12-h growth increment and the corresponding MTBS fire perimeter. Only increments with at least 50% overlap with MTBS were included in the analysis. This threshold retained 84% of the total spread increment dataset (n=47,098), demonstrating broad agreement between FEDS and MTBS despite more than an order of magnitude difference in the spatial resolution of their source data (375-m vs 30-m, respectively).

Predictive modeling of vegetation burn severity

We developed two models to explore the potential to predict final MTBS burn severity class using FEDS data, where we tested different versions of the decision tree-based ensemble model, XGBoost (Chen & Guestrin 2016)—a model with recent applications in studies related to burn severity and remote sensing (e.g., He et al. 2024; Seydi et al. 2024). The first (multiclass) model predicted the median MTBS class within each increment of growth, and the second (binary) model provided the probability that the median MTBS class within each increment was moderate/high severity (1) or not (0).

Each model was trained via a grid search, varying the decision tree count from 25 to 1000 and tree depth from 1 to 5. This strategy was chosen to achieve reasonable performance while being sensitive to overfitting and diminishing returns of continued model training. Input features included growth increment spread rate, the number of unique detection periods, the most commonly occurring LANDFIRE EVT value, designation of initial AM or PM observation, and FRP characteristics summarized as the mean, maximum, and area-normalized total (sum) on both the day of initial spread and over the lifetime of the fire. LANDFIRE EVT data included the four-digit EVT code, in addition to the simplified "EVT_ LF" and "EVT_PHYS" variables. Lastly, the ecoregion in which the fire occurred—as defined by Olson et al. (2001)—was included to provide a secondary, regional representation of ecological context. For each classification scheme (multiclass or binary), we compared models with three different sets of input variables: (1) a model with EVT and ecoregion characteristics only; (2) a model with active fire characteristics only; and (3) a model with the combination of all characteristics.

Similar to the area-based filtering threshold used for the data analysis, model training data included spread increments with at least 50% overlap with MTBS perimeters from fires occurring between 2012 and 2020 (n=39,460, across 1949 wildfires) with testing occurring on fires in 2021 (n=9000, across 221 wildfires). Evaluation metrics included accuracy, precision, recall, f1-score, and the area under the curve (AUC, binary only). No overlap criteria were applied to the testing data to simulate NRT application, consistent with higher expected uncertainty regarding up-to-date reference perimeter data availability at the time of satellite acquisition.

Results

Active fire properties and burn severity

At the event level, filtered and matched FEDS fires between 2012 and 2021 (n=2177, Fig. 1) in the western U.S. primarily burned conifer forests (76%), with smaller contributions from areas dominated by shrublands (14%) and grasslands (3.3%). Within each dominant vegetation type, median MTBS class values and FRP for each 12-h growth increment were positively correlated (Fig. 3, Table 1). In spread increments dominated by conifer forests, median total FRP per unit area (MW/km²) was 28% higher in areas designated as high burn severity (4) as compared to moderate severity (3) (Fig. 3a). This difference was even greater when comparing the distribution of mean FRP values for each increment, where FRP in high severity spread increments was 41% higher than in moderate severity increments (Fig. 3b). Overall, distributions of both the mean and area-normalized total FRP values for conifer spread increments were statistically different when comparing neighboring severity classes (Mann–Whitney *U* test, two-sided, p < 0.01).

Shrubland and grassland dominated fire growth increments exhibited similar relationships between FRP and MTBS burn severity (Fig. 3a-b, Table 1). For both vegetation types, the stepwise positive relationship between mean FRP and burn severity was more consistent than for area normalized total FRP. Shrublands had the highest mean FRP per burn severity class of the three vegetation types, consistent with evidence for hotter fires in shrub ecosystems based on fuel characteristics (e.g., Burger & Bond 2015; De Luis et al. 2004; Keeley et al. 1999). Mean FRP was not statistically different between high and moderate MTBS classes in shrublands or grasslands. Small sample sizes for high burn severity increments in grasslands and shrublands may partially contribute to this finding (see Table 1); heterogeneity in vegetation cover may also lead to less consistent relationships between FRP and burn severity in grasslands. Notably, metrics of total FRP exhibited greater differences across class categories when grouped into unburned/low (1 and 2) and

Orland et al. Fire Ecology (2025) 21:55 Page 7 of 18

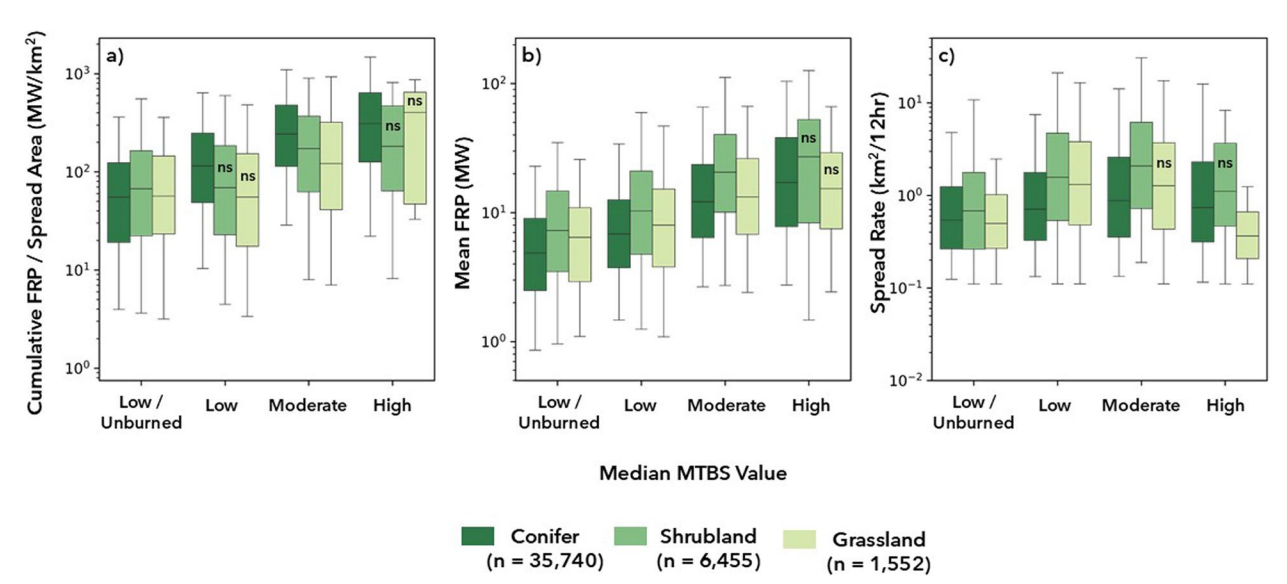


Fig. 3 FEDS properties delineated by dominant vegetation type and MTBS burn severity class. "ns" designation indicates non-significant variable difference between the assigned burn severity class and the measurements in the class directly below it. **a** Area normalized cumulative FRP measurements, per increment, over the lifetime of the fire. Mean increment FRP values over the lifetime of the fire. **c** 12-h spread rate as measured by the increment's area. Whiskers represent the 5th and 95th percentiles, and outliers are not shown

moderate/high (3 and 4) severity classes, illustrating the potential to tailor NRT metrics to support specific information needs for emergency response.

Higher MTBS severity consistently corresponded to faster spread rates for conifer and shrubland vegetation types from unburned/low (0) to moderate (3) severity (Fig. 3c). For shrubland-dominant increments, those classified at high (4) severity (n=39) were not considered statistically different from moderate severity (n = 1206). Differences between sample sizes likely affect these results. For conifers, median spread rates were marginally slower at high severity (0.74 km²/12 h) vs moderate severity (0.88 km²/12 h), and these differences were statistically different. For grassland environments, rates of spread increased between the unburned/low (1) and low (2) severity classes, and differences between the moderate (3) and low (2) categories were not statistically different. Median spread rates declined by 71%—the highest among all classes—between moderate and high severity categories. In addition to the limited sample size in the highest severity class (n = 12), the 12-h revisit time of the VIIRS sensor may not be sufficient to capture the fastmoving nature of grassland fires.

Differences in fire behavior by vegetation type underscore the value of fire tracking for assessing ecological impacts of fire activity (Fig. 4). For example, shrubland and grassland fires spread faster than fires in coniferdominated landscapes (Fig. 4a). The median values of VIIRS-based spread rates for grassland and shrubland classes were 53% and 106% higher, respectively, than for

fire spread increments in conifers. Conifer-dominated growth increments burned longer than those dominated by other vegetation types, with median fire persistence of five 12-h periods (Fig. 4b). Fire persistence was also more variable in conifer forests, measured as the hours between the first and last active fire pixel within each increment (Fig. 4c), where the median duration was 96 h (interquartile range: 168 h) compared to 12 h in both shrubland and grassland spread increments (interquartile range: 60 h). As such, more persistent fire activity in conifer environments boosted total FRP per unit area, consistent with the expected influence of elevated fuel loading, fuelbed depth, and fuel particle heat content in forested ecosystems on fire behavior (Rothermel 1972).

The influence of initial versus extended MTBS assessment type on the relationship between burn severity and metrics of fire behavior varied by vegetation type. Estimated burn severity for conifer increments was largely sourced from extended assessments (n = 30,345of 35,740, or 85%). As a result, the relationships between burn severity and fire behavior metrics were comparable between extended assessments (Fig. S1) and the combined data shown in Fig. 3. For conifer increments with initial assessment data, the overall patterns remain unchanged, but the distributions of mean FRP and fire spread rate were higher across all severity classes than in the combined dataset (Fig. S2). By contrast, most MTBS data for shrubland and grassland growth increments were drawn from initial assessments (58% and 60%, respectively). For shrublands, the overall relationships were

Table 1 Differences in spread rate, area normalized total FRP, and mean FRP across conifer, shrubland, and grassland environments for each MTBS class

		Spread rate (km ² /12 h)	n²/12 h)		Total FRP/spre	Total FRP/spread area (MW/km²)	m²)	Mean FRP (MW)	W)		
		5th percentile	50th percentile	95th percentile	5th percentile	50th percentile	95th percentile	5th percentile	e 50th percentile	95th percentile	Sample size
Dominant vegetation type	Median MTBS class										
Conifer	Low/ unburned (1)	0.12	0.54	4.84	3.96	55.48	362.41	0.86	4.87	22.97	2112
	Low (2)	0.13	0.71	7.49	10.39	115.01	639.6	1.47	6.85	34.17	21,205
	Moderate (3)	0.13	0.88	14.19	28.72	243.06	1101.3	2.66	12.17	65.98	10,672
	High (4)	0.12	0.74	16.01	22.05	310.62	1478.78	2.73	17.14	104.36	1751
Shrubland	Low/ unburned (1)	0.11	0.68	10.82	3.64	67.19	557.51	96.0	7.27	36.21	513
	Low (2)	0.11	1.57	21.13	4.48	69.07	299.68	1.25	10.32	59.77	4697
	Moderate (3)	0.18	2.08	30.78	7.97	173.39	905.88	2.71	20.54	112.93	1206
	High (4)	0.11	1.11	8.43	8.17	182.41	849.17	1.44	27.11	126.31	39
Grassland	Low/ unburned (1)	0.11	0.5	2.55	3.16	56.75	384.46	96.0	6.44	26.97	185
	Low (2)	0.11	1.31	16.57	3.36	55.51	482.89	1.09	8.01	47.04	1151
	Moderate (3)	0.11	1.27	17.53	6.97	121.49	1041.39	2.18	13.24	74.35	204
	High (4)	0.1	0.37	11.76	20.7	403.34	1688.52	1.94	15.35	83.4	12

Orland et al. Fire Ecology (2025) 21:55 Page 9 of 18

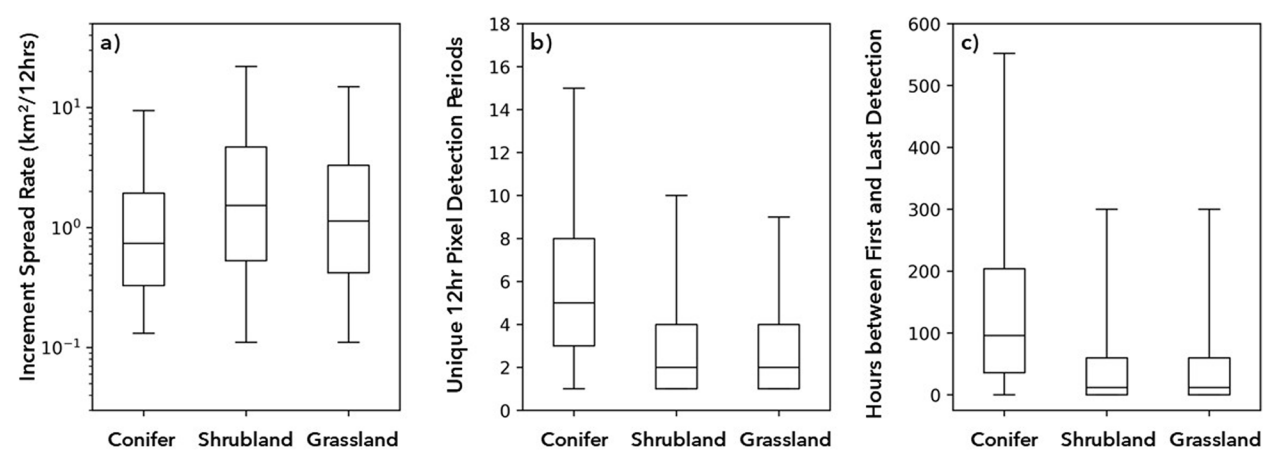


Fig. 4 a Distributions of increment spread rate for all fires stratified by dominant vegetation type (km²/12 h). **b** Distributions of the number of unique periods in which one or more VIIRS pixel(s) were detected within an individual spread increment, stratified by dominant vegetation type. **c** Distribution of the hours between the first and last active fire detections within a spread increment, stratified by dominant vegetation type. Whiskers represent the 5th and 95th percentiles, and outliers are not shown

consistent between initial assessment data and the combined dataset, but with a clearer separation of median fire intensity and higher spread rates by initial assessment class. Initial assessment data for grasslands also provided greater separability by burn severity class for mean FRP and cumulative FRP metrics. Remaining shrubland and grassland data sourced from extended assessments exhibited higher intensity measures and lower spread rates than those shown in (Fig. S1).

Diurnal behavior

The 12-h cadence of the VIIRS observations further allows for the comparison of differences in fire behavior metrics between nighttime and daytime overpasses, including differences in spread rate and intensity across severity classes. MTBS burn severity class distributions separated by AM/PM overpass designation were statistically different from one another (p < 0.01), where spread increments tied to PM VIIRS active fire detections exhibited higher severity classes overall. Indeed, when limiting normalized total FRP values to only the time of the initial VIIRS overpass, intensity values were consistently higher for initial PM observations than initial AM observations across all vegetation types and burn severity classes (Fig. 5a-c). Observed differences between AM and PM VIIRS overpasses are consistent with the expected diurnal cycle of fire intensity, with more intense burning during afternoon hours due to higher temperatures, lower relative humidity, and often higher wind speeds (Andela et al. 2015; Giglio 2007).

Integrating over the lifetime of each fire event resulted in more even estimates of FRP (Fig. 5d-f). Considering the full lifetime of the fire, the ratio of PM/AM

cumulative FRP aggregated across all increments varied by a factor of approximately two or less in conifer systems, with higher observed ratios in shrubland (approximately 2–4×) and grassland (approximately 3×, excluding outliers) ecosystems (Table 2). For conifers, high severity increments were relatively evenly distributed across both periods of morning and afternoon growth, highlighting the influence of fire persistence on burn severity, where longer duration burning leads to more complete fuel consumption in higher fuel load systems. Conversely, the time of initial fire spread may have a stronger influence on burn severity in shrubland and grassland ecosystems—especially those considered for initial assessments only.

We also observed diurnal variation in spread rates, with larger afternoon spread across nearly all burn severity classes (Fig. 6a-c). In conifer forests, elevated afternoon fire spread rates are consistent with expected behavior and supported by the strong differences in the initial AM and PM FRP measurements. For example, higher PM (13:30) FRP values track daily meteorological conditions (e.g., higher temperatures and lower humidity) amenable to greater afternoon (13:30 to 01:30) fire spread. Furthermore, the increasing ratio between afternoon and morning spread rates across MTBS classes in conifer environments points to the contributions of diurnal variability in behavior on burn severity, where higher burn severity classes are observed to coincide with periods of increasingly faster afternoon spread (Fig. 6d). For shrublands burned at moderate severity, afternoon spread rates were about one and a half times as fast as morning spread rates (Fig. 6e), before dropping to below 1×at the highest severity class. This subsequent decrease may be the

Orland et al. Fire Ecology (2025) 21:55 Page 10 of 18

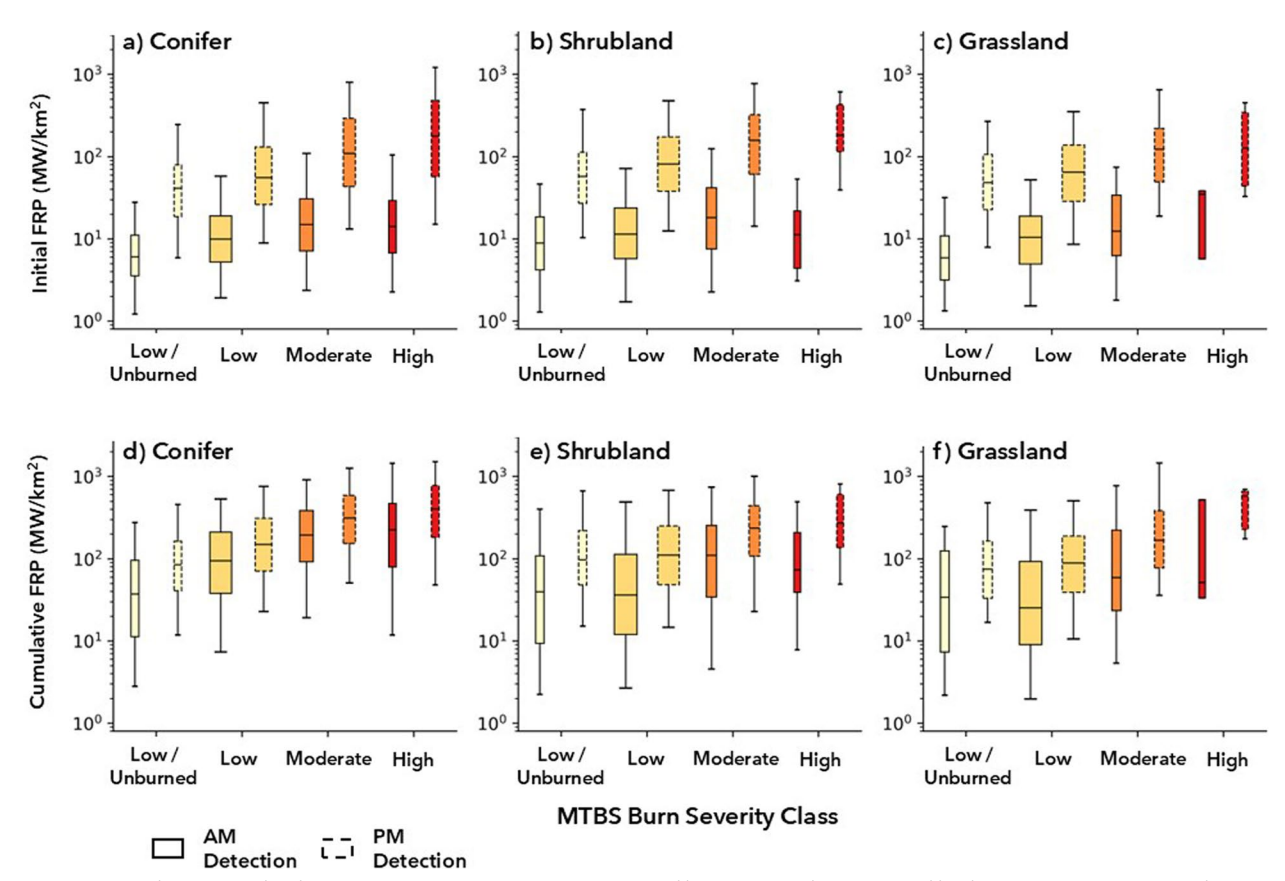


Fig. 5 a–c Initial area normalized FRP measurements per vegetation type and burn severity class, separated by the overpass time associated with each spread increment (AM, 01:30; PM, 13:30). d–f Cumulative area normalized FRP considering all detections observed within the spread increment over the lifetime of the fire, stratified by overpass time for initial spread increment delineation. The total number of spread increments differed by dominant vegetation type: conifer (n=35,740), shrubland (n=6455) and grassland (n=1552)

Table 2 Ratio of median Initial and Cumulative FRP for PM (13:30) and AM (01:30) spread increments for each vegetation type and burn severity class. The full distributions for initial and cumulative FRP by overpass time are shown in Fig. 5

Vegetation type	MTBS class	PM:AM FRP ratio		
		Initial	Cumulative	
Conifer	Low/unburned (1)	6.8	2.3	
	Low (2)	5.6	1.6	
	Moderate (3)	7.3	1.6	
	High (4)	12.6	1.8	
Shrubland	Low/unburned (1)	6.4	2.5	
	Low (2)	7.1	3.1	
	Moderate (3)	8.7	2.1	
	High (4)	16.2	3.7	
Grassland	Low/unburned (1)	8.2	2.2	
	Low (2)	6.2	3.5	
	Moderate (3)	9.9	2.8	
	High (4)	3.7	11.2	

result of small sample size (n=39). By contrast, afternoon and morning fire spread rates were more comparable in grasslands between low and moderate severity classes (Fig. 6f), while spread rates at the highest severity class were over twice as fast during the afternoon. This pattern suggests that fire intensity may be a stronger control on burn severity between low and moderate classes in grassland environments, and where the limited sample size at high severity (n=12) makes further interpretation difficult.

Burn severity prediction via supervised machine learning

Metrics of fire behavior from FEDS tracking contributed to successful predictions of MTBS burn severity (Table 3). For both multiclass and binary prediction, models that combined vegetation and active fire data showed improved performance over models that considered these categories of variables separately. Multiclass accuracy reached a maximum of 67% considering both variable categories, 64% considering vegetation data only, and 65% considering active fire metrics only.

Orland et al. Fire Ecology (2025) 21:55 Page 11 of 18

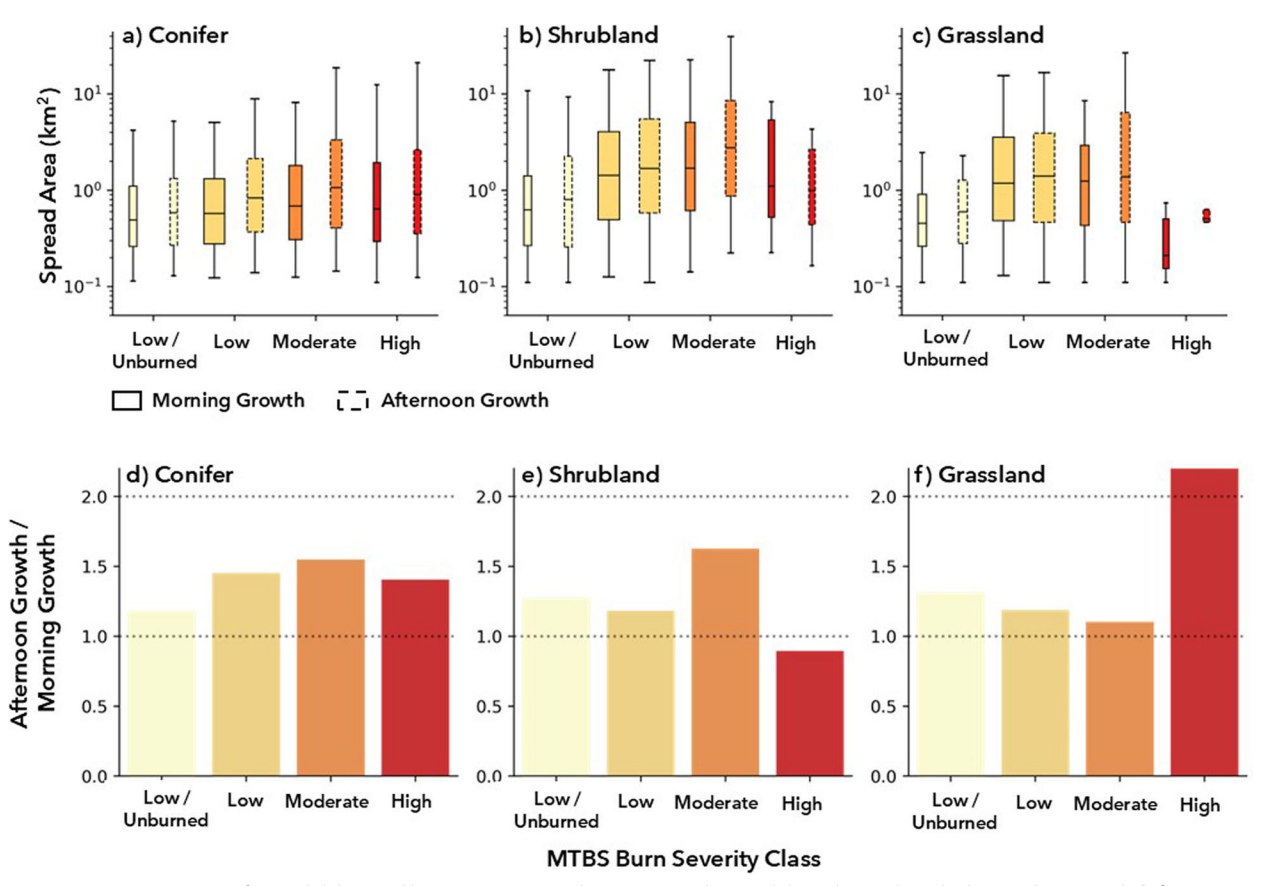


Fig. 6 a–c Increment rate of spread delineated by vegetation type, burn severity class, and diurnal period in which growth occurred. d–f Ratio between median afternoon growth values and median morning growth values separated by vegetation type and burn severity class

Table 3 Results from the best performing multiclass and binary models, both of which used all variable input types. Details on tree count and depth are also provided

	Output type: median MTBS value	Precision	Recall	F-1 score	Sample size per class
Multiclass prediction	Unburned/low (1)	0.49	0.05	0.09	870
Trees = 250	Low (2)	0.7	0.88	0.78	5,723
Depth=3	Moderate (3)	0.52	0.43	0.47	2,109
	High (4)	0.21	0.02	0.04	298
	Accuracy	67%			Total sample size
	Total area correctly predicted	16,101 km² (69%)			9000
Binary prediction	Unburned/low (1/2)	0.83	0.88	0.86	6593
Trees = 100	Moderate/high (3/4)	0.61	0.5	0.55	2407
Depth=5	Accuracy	78%			Total sample size
	AUC	0.69			9000
	Total area correctly predicted	17,944 km² (76%)			

Similarly, binary class accuracies were even higher at 78% (AUC=0.69), 74% (AUC=0.59), and 76% (AUC=0.63) for these same categories of values, respectively. Although overall model accuracies were similar in each scenario, including active fire information specifically

improved model performance for moderate/high severity classification (3 or 4), which peaked with the combination of vegetation, ecoregion, and active fire data. The optimally performing models also varied by vegetation type. For instance, binary AUC results were highest for

Orland et al. Fire Ecology (2025) 21:55 Page 12 of 18

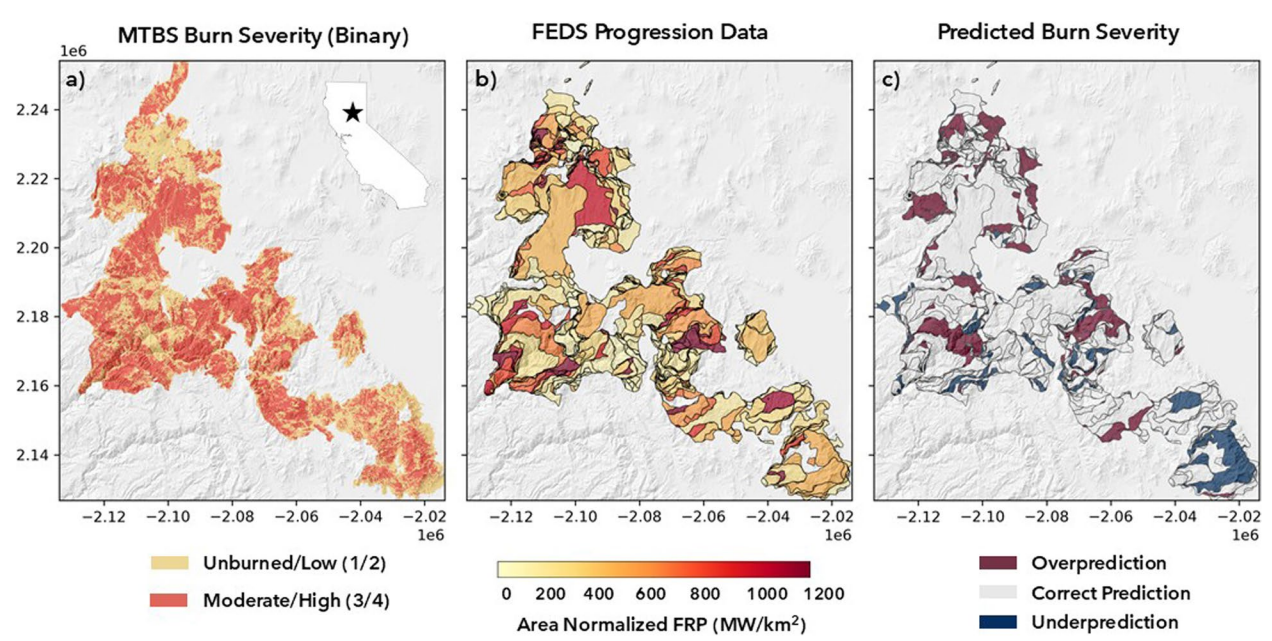


Fig. 7 a MTBS burn severity data with hillshade overlay for the 2021 Dixie and Sugar Fires. **b** FEDS growth increments colored by cumulative area normalized total FRP (MW/km²). **c** Binary prediction results using the XGBoost model with all input features. The binary median MTBS severity category is correctly predicted for all areas in gray; those colored in red and blue represent model overpredictions and underpredictions, respectively. 74% of the total tracked area is correctly predicted by the model. Data are shown in native MTBS projection (Albers Equal Area Conic) with linear units in meters

conifer spread increments (0.69), lower for shrublands (0.56), and lowest for grasslands (0.52), where an imbalance in the training data between low and high severity may lower AUC values in shrublands and grasslands. An analysis using models that only included active fire information at the initial satellite overpass time showed reduced performance for conifers (AUC=0.65), but comparable performance for shrubland (AUC=0.55) and grassland (AUC=0.50) environments.

The best performing multiclass and binary models correctly classified 69% and 76% of the total 23,461 km² of fire-affected area in the testing dataset, respectively. For the approximately 18,000 km² of correctly predicted results from the binary model, the median time between the first and last detection was 72 h, allowing for timely estimates of burn severity for growth increments in a larger fire before fire containment. For systems with lower fuel loads, "day of" active fire detections may provide sufficient information to deliver model estimates within hours of initial detection. Figure 7 highlights model results for the Dixie and Sugar fires—a long-lasting wildfire complex with a large high severity component, which burned in northern California from July to October in 2021. The binary class model correctly classified 74% of the total burned area mapped by MTBS, with a median period of 84 h (3.5 days) between the first and last detections within each FEDS-tracked increment of fire growth. These results illustrate the potential to deliver initial predictions of burn severity in NRT.

Discussion

Linkages between metrics of fire behavior and burn severity

Near real-time metrics of fire intensity and behavior from satellite-based fire tracking were strongly correlated with post-fire burn severity for large fire events in the western U.S. between 2012 and 2021. The relationships between FRP and burn severity varied by vegetation type and overpass time, demonstrating the ability of the VIIRS sensor and FEDS algorithm to capture Key differences in fire behavior that alter burn severity over 12-h increments of fire growth. These results highlight the potential to refine and extend this approach to provide situational awareness before a large fire is contained or suppressed, where NRT indicators of burn severity derived from metrics of fire behavior can complement traditional approaches that rely on changes in surface reflectance (e.g., dNBR).

Specifically, our results demonstrate that higher FRP values were consistently associated with higher MTBS severity classifications. While these relationships were strongest for fires in conifer forests, these broad patterns were also evident in shrublands and grasslands. Our findings build upon previous work using active fire

Orland et al. Fire Ecology (2025) 21:55 Page 13 of 18

observations from MODIS or geostationary sensors to investigate the relationships between fire intensity and biomass consumption (Li et al. 2018) or burn severity (Chatzopoulos-Vouzoglanis et al. 2024; Heward et al. 2013; Ponomarev et al. 2023), with our work drawing upon the higher spatial resolution of VIIRS-based fire tracking methods to establish quantitative relationships between fire intensity and MTBS severity designations for individual growth increments. The relationships between fire intensity and burn severity were also consistent across multiple assessment timeframes, demonstrating linkages between both immediate and delayed effects. Results from both assessment types further contextualize the range of expected fire behavior for a given vegetation type across varied ecosystems. For instance, sparse conifer forests may only have an initial MTBS assessment designed to capture immediate fire impacts, yet active fire observations indicating persistent and/or high-intensity burning may indicate elevated risk for secondary effects such as delayed tree mortality. This information may assist land managers with decisions conventionally aided by extended assessment data, including targeting the removal of dead woody fuels or prioritizing locations for reseeding if the environment displays low seed source connectivity.

Our study also provides a quantitative assessment of the relationships among fire spread, fire persistence, and burn severity across three major vegetation types. Overall, fire spread rate and burn severity were positively correlated across cover types, except in spread increments classified at the highest severity level. The additional consideration of fuel load may help explain deviations from this pattern. For instance, fire growth increments in conifer forests burned several times longer than in shrubland or grassland ecosystems, and our results suggest that integrated measures of FRP over several VIIRS overpasses were more consistent predictors of high burn severity in these systems. These findings are in line with observations by Birch et al. (2014) in Northern Rocky Mountain forests that daily burned area growth was only weakly correlated with high burn severity. Hantson et al. (2022) nonetheless found that the rate of spread derived using VIIRS active fire detections indeed had positive correlations with both FRP and tree mortality in California. Differences in forest type, measures of severity, and fire tracking methods may contribute to the inconsistent conclusions between studies, as well as how tailoring FEDS tracking approaches to individual regions can provide enhanced predictions of burn severity that account for the complexities within specific environments. Future work to investigate the role of spread rate is additionally needed to resolve the potential confounding effects of observed differences in morning and afternoon growth in this study. As such, continued investigations into both the drivers and impacts of high intensity fire growth may assist practitioners with key decisions related to fireline suppression, evacuation planning, and related response efforts on emergency timelines.

The predictive power and utility of NRT tracking

The results in this study highlight the potential for NRT fire tracking to provide rapid assessments of burn severity within hours after each satellite overpass. Models that included behavior metrics were more accurate than those that considered vegetation alone, with an overall accuracy of 78% for the binary separation of moderate/high and unburned/low severity classes for 221 wildfires in 2021. Machine learning model results using exclusively NRT metrics and pre-fire vegetation data were consistent predictors of burn severity in lower fuel load systems, demonstrating the ability to provide decision support in these ecosystems within hours of initial detection. By contrast, cumulative measures of FRP were important modifiers of burn severity in conifer forests measured over successive VIIRS overpass periods, highlighting the potential benefits from an approach that iteratively updates severity estimates as new information is received. Our results from the Dixie and Sugar fires (Fig. 7) demonstrate the applicability of these methods for incidents which lasted for several months, where model predictions can provide provisional information on burn severity for situational awareness until higher resolution burn severity datasets become available. The use of empirical predictive models based on pre- and active fire data can serve as an additional tool for assessing fire impacts, where the cadence of NRT data availability can complement other modeling approaches (Anderson 1982; Scott & Burgan 2005; Staley et al. 2018; Wells et al. 2023).

Continued refinement and adoption of NRT fire tracking may additionally assist partner agencies with their operational and planning goals, where iterative product development can be tailored to meet individual stakeholder needs. For instance, the expedited delivery and analysis of FEDS data supports priority areas within the United States Forest and Rangelands National Strategy (2014), such as those focused on assessing fire intensity during an event and measuring response efforts based on observed fire behavior. Indicators of burn severity from NRT fire tracking may also support selective non-intervention strategies that allow for monitored, low-intensity fire spread to reduce fuel loads, while identifying rapid and/or high-intensity growth which may necessitate more interventional responses. Similarly, U.S. Forest Service Wildfire Crisis Implementation Plan (2022) emphasizes the need for continued fuels treatments across multiple jurisdictional boundaries, as well as the importance of reforestation Orland et al. Fire Ecology (2025) 21:55 Page 14 of 18

efforts within burn scars. For each of these goals, FEDS NRT tracking data and derived indicators of burn severity may contribute information across the fire lifecycle. For example, pre-fire fuel treatments could target areas adjacent to low-intensity burning, providing greater spatial continuity of reduced fuel loads. Active fire tracking may also support BAER teams with mapping anticipated ecological impacts linked to soil burn severity. Given that extended MTBS severity assessments are typically delivered 1 year following a fire event, burn severity indicators from NRT fire tracking may also contribute early guidance for targeting logging and reseeding efforts in the post-fire environment. Finally, direct integration of FEDS data with U.S. Forest Service Potential Operation Delineations (POD) boundaries (Calkin et al. 2021; O'Connor et al. 2017; Thompson et al. 2022) may further inform the success of future suppression efforts, where records of fire behavior can provide greater context for evaluations of prior suppression outcomes (e.g., Young et al. 2024).

Future directions

Beyond the initial demonstration in this study, there are several possible pathways to further improve modeled burn severity based on indicators derived from fire tracking data. The inclusion of additional information on topography, fuels, and fire weather during each 12-h growth increment may improve modeled burn severity, particularly in mountainous regions or during weather extremes that modify relationships between fire behavior and severity. Additional active fire information, either from current or future satellite and airborne systems, could also improve the representation of fire spread, persistence, and intensity needed to capture fine-scale heterogeneity in burn severity (Liu et al. 2024). Similarly, evidence for increasing fire intensity during overnight hours (Balch et al. 2022; Luo et al. 2024) supports continued investigations into nighttime FRP and fire persistence as potential drivers of higher fire severity in future events.

Satellite-based fire tracking may also support the development and evaluation of other NRT metrics of burn severity, including categorical or continuous metrics related to soil burn severity. Future work to integrate fire persistence, total FRP, active fire line characteristics (Chen et al. 2022), and measured soil impacts could provide a pathway to expand upon previous studies of soil burn severity in laboratory or small-scale settings. For instance, surface burning induces soil water repellency, but repellency can also be destroyed beyond a critical intensity—duration heating threshold (Debano 2000; Doerr et al. 2004; Letey 2001). With a path laid out by prior laboratory studies (e.g., Robichaud & Hungerford 2000), continued work to couple field measurements with total wildfire energy output and fire persistence via

remote sensing may provide further insight regarding the heterogeneity of soil impacts from wildfires—including the related risk of post-fire hydrologic hazards such as flash flooding or debris flows, as well as longitudinal impacts to water quality from eroded sediment and ash. Current and future satellite lidar and radar observations may also provide complementary information on changes in vegetation structure and moisture to refine estimates of fine-scale variability in vegetation and soil burn severity within large fire events to complement metrics from sub-daily fire tracking such as FEDS.

Finally, growing awareness of the importance of fire behavior may motivate the consideration of additional NRT estimates of fire impacts not regularly considered by national mapping programs such as MTBS or BAER. For example, recent work by Balch et al. (2024) linked rapid fire spread to a higher number of damaged structures. Faster fires pose unique threats to communities and firefighters, and traditional spectral indices for burn severity (e.g., dNBR and NDVI) may not be suitable to characterize infrastructure damages in the wildland urban interface. Thus, NRT metrics of fire behavior provide an additional line of evidence to support the rapid assessment of fire impacts in both human-dominated and natural landscapes.

Uncertainties in fire detection

VIIRS active fire detections provide NRT information to assess individual fire behavior and estimate burn severity, yet the 12-h cadence of VIIRS observations may not capture critical burning times. For instance, the diurnal cycle of fire activity in the western U.S. typically peaks in the mid to late afternoon, with a decay in energy during the nighttime (Giglio 2007; Mu et al. 2011). Wiggins et al. (2020) additionally found significant variations in diurnal cycle activity across multiple fires and land cover types. As a result, VIIRS overpass times in the early afternoon and early morning hours may not capture critical periods of fire intensity needed to characterize burn severity. Similarly, growth increments between the VIIRS overpass times mix daytime and nighttime fire spread. Along with the growing recognition of the impacts of climate change on the diurnal cycle of fire activity (e.g., Balch et al. 2022; Luo et al. 2024), fire tracking based on VIIRS overpass times may not be sufficient for capturing distinct differences in daytime and nighttime behavior. New fire tracking and analysis efforts from geostationary satellites (e.g., Li et al. 2022; Liu et al. 2024) may provide a basis for estimating variability in fire intensity between VIIRS overpasses, along with data from future missions such as WildFireSat (Johnston et al. 2020). Finally, several additional factors may also influence satellite-based FRP, such as the presence of clouds or dense smoke cover, daily changes in pixel resolution related to view angle, or

Orland et al. Fire Ecology (2025) 21:55 Page 15 of 18

spurious detections. Future work to correct the atmospheric attenuation of fire energy—as well as considering the VIIRS sensors on the NOAA20 and NOAA21 satellites for more consistent observations—may help clarify the underlying relationships between fire intensity and burn severity and advance approaches to leverage NRT data for operational uses.

Conclusions

We ran the FEDS algorithm (Chen et al. 2022) across the western U.S. to compare fire behavior and burn severity for all large fires from 2012 to 2021. Our findings confirm consistent positive relationships between satellitederived estimates of FRP and categorical assessments of burn severity. Additional metrics of fire spread and fire persistence capture differences in fire behavior that modify burn severity for the dominant land cover types in the western U.S. The capability to run the FEDS algorithm in NRT underscores the possibility to estimate burn severity for each 12-h growth increment within hours after each satellite overpass. Therefore, we anticipate that the resulting data streams can contribute to situational awareness about the impacts of an ongoing fire, including how low intensity burning may assist with resource management objectives and planning of future fuels treatments. In collaboration with operational partners, there are opportunities to tailor and improve this modeling approach based on the integration of additional fire detection information from VIIRS or other airborne or satellite sensors, as well as ancillary data to target specific NRT information needs. This same approach to link fire behavior and fire impacts could also provide a path to estimate soil burn severity or other post-fire measures, where NRT data could complement existing products in the western U.S. or other regions with mapped severity data.

Supplementary Information

The online version contains supplementary material available at https://doi.org/10.1186/s42408-025-00407-x.

Supplemental Figure S1. FEDS properties delineated by dominant vegetation type and MTBS burn severity class for extended assessments only.

a) Area normalized cumulative FRP measurements, per increment, over the lifetime of the fire. b) Mean increment FRP values over the lifetime of the fire. c) 12-h spread rate as measured by the increment's area. Markers indicate median values across all assessment types. For further comparison, refer to Fig. 3.

Supplemental Figure S2. FEDS properties delineated by dominant vegetation type and MTBS burn severity class for initial assessments only. a) Area normalized cumulative FRP measurements, per increment, over the lifetime of the fire. b) Mean increment FRP values over the lifetime of the fire. c) 12-h spread rate as measured by the increment's area. Markers indicate median values across all assessment types. For further comparison, refer to Fig. 3

Acknowledgements

The authors are grateful to Greg Corradini, Julia Signell, Alex Mandel, Sujen Shah, and the rest of the NASA VEDA team for their assistance with the development and production of the FEDS data. The authors are also grateful to Francis Rengers for his input and support on this project, as well as to Andrew Graber and two anonymous reviewers for their constructive feedback on the manuscript.

Authors' contributions

EO contributed to the project conception, algorithm development, data generation, and primary data analysis. DCM and MFC contributed to project conception and supervision. TM, YC, RS, ZB, and AS contributed to data generation and algorithm development. KN, BP, and RL contributed to project conception and advising. SC, TL, JR, and all co-authors contributed to writing.

Funding

This project was funded by NASA's Wildland Fire Applied Sciences Program (EO, DCM), Earth Information System (EIS) Project (MFC, TDM, ANS, SRC), and the Modeling Analysis and Prediction (MAP) Program (YC). Any use of trade, product, or firm names is for descriptive purposes only and does not imply endorsement by the U.S. Government.

Data availability

FEDS data and analysis workflows used in this manuscript are available at the following repository link: https://doi.org/10.5281/zenodo.15261835.
MTBS data can be downloaded from https://www.mtbs.gov/. LANDFIRE data are available at https://landfire.gov/. The current production and development branches of the FEDS algorithm are available at: https://github.com/Earth-Information-System/fireatlas. Near real-time VIIRS data are available from NASA FIRMS: https://firms.modaps.eosdis.nasa.gov. Near real-time FEDS fire perimeter data are available at: https://openveda.cloud/api/features/. Documentation for API access is available at the following link: https://docs.openveda.cloud/user-guide/notebooks/tutorials/mapping-fires.html. FEDS data for the current year are available for download and visualization as part of NASA's Fire Event Explorer tool: https://earthdata.nasa.gov/dashboard/tools/fire-event-explorer.

Declarations

Ethics approval and consent to participate

Not applicable.

Consent for publication

Not applicable.

Competing interests

The authors have no competing interests.

Author details

¹NASA Goddard Space Flight Center, Greenbelt, MD, USA. ²University of Maryland Baltimore County, GESTAR II, Baltimore, MD, USA. ³University of Maryland College Park, College Park, MD, USA. ⁴University of California Irvine, Irvine, CA, USA. ⁵U.S. Geological Survey, Alaska Science Center, Anchorage, AK, USA. ⁶University of British Columbia, Vancouver, BC, Canada. ⁷US Geological Survey Earth Resources Observation and Science Center, Sioux Falls, SD, USA.

Received: 10 September 2024 Accepted: 23 August 2025 Published online: 07 October 2025

References

Abatzoglou, J. T., and A. P. Williams. 2016. Impact of anthropogenic climate change on wildfire across western US forests. *Proceedings of the National Academy of Sciences of the United States of America*. https://doi.org/10.1073/pnas.1607171113.

Adams, M.A. 2013. Mega-fires, tipping points and ecosystem services: Managing forests and woodlands in an uncertain future. Forest Ecology and Management 294: 250–261. https://doi.org/10.1016/j.foreco.2012.11.039. Orland et al. Fire Ecology (2025) 21:55 Page 16 of 18

- Ahmad, S.K., T.R. Holmes, S.V. Kumar, T.M. Lahmers, P.-W. Liu, W. Nie, A. Getirana, E. Orland, R. Bindlish, A. Guzman, C.R. Hain, F.S. Melton, K.A. Locke, and Y. Yang. 2024. Droughts impede water balance recovery from fires in the Western United States. *Nature Ecology & Evolution* 8 (2): 229–238. https://doi.org/10.1038/s41559-023-02266-8.
- Alexakis, D., I. Kokmotos, D. Gamvroula, and G. Varelidis. 2021. Wildfire effects on soil quality: Application on a suburban area of West Attica (Greece). *Geosciences Journal* 25 (2): 243–253. https://doi.org/10.1007/s12303-020-0011-1.
- Andela, N., J.W. Kaiser, G.R. Van Der Werf, and M.J. Wooster. 2015. New fire diurnal cycle characterizations to improve fire radiative energy assessments made from MODIS observations. *Atmospheric Chemistry and Physics* 15 (15): 8831–8846. https://doi.org/10.5194/acp-15-8831-2015.
- Andela, N., D.C. Morton, L. Giglio, R. Paugam, Y. Chen, S. Hantson, G.R. Van Der Werf, and J.T. Randerson. 2019. The global fire atlas of individual fire size, duration, speed and direction. *Earth System Science Data* 11 (2): 529–552. https://doi.org/10.5194/essd-11-529-2019.
- Andela, N., Morton, D.C., Schroeder, W., Chen, Y., Brando, P.M., and Randerson, J.T. 2022. Tracking and classifying Amazon fire events in near real time. Science Advances, 8(30):eabd2713. https://doi.org/10.1126/sciadv.abd2713
- Anderson, H.E. 1982. Aids to determining fuel models for estimating fire behavior.

 U.S. Department of Agriculture, Forest Service, Intermountain Forest and Range Experiment Station. https://doi.org/10.2737/int-gtr-122
- Archibald, S., and Roy, D.P. 2009. Identifying individual fires from satellitederived burned area data. 2009 IEEE International Geoscience and Remote Sensing Symposium, III-160-III-163. https://doi.org/10.1109/IGARSS.2009. 5417974
- Balch, J.K., St. Denis, L.A., Mahood, A.L., Mietkiewicz, N.P., Williams, T.M., McGlinchy, J., and Cook, M.C. 2020. Fired (Fire events delineation): An open, flexible algorithm and database of us fire events derived from the modis burned area product (2001–2019). Remote Sensing, 12(21):1–18. https://doi.org/10.3390/rs12213498
- Balch, J. K., B. A. Bradley, C. M. D'Antonio, and J. Gómez-Dans. 2013. Introduced annual grass increases regional fire activity across the arid western USA (1980–2009). *Global Change Biology* 19 (1): 173–183. https://doi.org/10.1111/qcb.12046.
- Balch, J. K., J. T. Abatzoglou, M. B. Joseph, M. J. Koontz, A. L. Mahood, J. McGlinchy, M. E. Cattau, and A. P. Williams. 2022. Warming weakens the night-time barrier to global fire. *Nature* 602 (7897): 442–448. https://doi.org/10.1038/s41586-021-04325-1.
- Balch, J.K., V. Iglesias, A.L. Mahood, M.C. Cook, C. Amaral, A. DeCastro, S. Leyk, T.L. McIntosh, R.C. Nagy, L. St. Denis, T. Tuff, E. Verleye, A.P. Williams, and C.A. Kolden. 2024. The fastest-growing and most destructive fires in the US (2001 to 2020). Science 386 (6720): 425–431. https://doi.org/10.1126/ science.adk5737.
- Birch, D.S., P. Morgan, C.A. Kolden, A.T. Hudak, and A.M.S. Smith. 2014. Is proportion burned severely related to daily area burned? *Environmental Research Letters* 9 (6): 064011. https://doi.org/10.1088/1748-9326/9/6/064011.
- Bond-Lamberty, B., S. D. Peckham, S. T. Gower, and B. E. Ewers. 2009. Effects of fire on regional evapotranspiration in the central Canadian boreal forest. *Global Change Biology* 15 (5): 1242–1254. https://doi.org/10.1111/j. 1365-2486.2008.01776.x.
- Bowman, D.M.J.S., J.K. Balch, P. Artaxo, W.J. Bond, J.M. Carlson, M.A. Cochrane, C.M. D'Antonio, R.S. DeFries, J.C. Doyle, S.P. Harrison, F.H. Johnston, J.E. Keeley, M.A. Krawchuk, C.A. Kull, J.B. Marston, M.A. Moritz, I.C. Prentice, C.I. Roos, A.C. Scott, Thomas W.. Swetnam, Guido R.. van der Werf, and S.J. Pyne. 2009. Fire in the Earth system. *Science* 324 (5926): 481–484. https://doi.org/10.1126/science.1163886.
- Burger, N., and W.J. Bond. 2015. Flammability traits of Cape shrubland species with different post-fire recruitment strategies. *South African Journal of Botany* 101: 40–48. https://doi.org/10.1016/j.sajb.2015.05.026.
- Calkin, D., C. O'Connor, M. Thompson, and R. Stratton. 2021. Strategic wildfire response decision support and the risk management assistance program. Forests 12 (10): 1407. https://doi.org/10.3390/f12101407.
- Cannon, S.H. 2001. Debris-flow generation from recently burned watersheds. Environmental and Engineering Geoscience. https://doi.org/10.2113/ gseegeosci.7.4.321.
- Cannon, S. H., and J. DeGraff. 2009. The increasing wildfire and post-fire debrisflow threat in western USA, and implications for consequences of

- climate change. *Landslides Disaster Risk Reduction*. https://doi.org/10. 1007/978-3-540-69970-5 9.
- Chatzopoulos-Vouzoglanis, K., K.J. Reinke, M. Soto-Berelov, and S.D. Jones. 2024. Are fire intensity and burn severity associated? Advancing our understanding of FRP and NBR metrics from Himawari-8/9 and Sentinel-2. *International Journal of Applied Earth Observation and Geoinformation* 127: 103673. https://doi.org/10.1016/j.jag.2024.103673.
- Chen, T., and C. Guestrin. 2016. XGBoost: A scalable tree boosting system. Proceedings of the ACM SIGKDD International Conference on Knowledge Discovery and Data Minina. https://doi.org/10.1145/2939672.2939785.
- Chen, Y., J. T. Randerson, G. R. Van Der Werf, D. C. Morton, M. Mu, and P. S. Kasibhatla. 2010. Nitrogen deposition in tropical forests from savanna and deforestation fires. *Global Change Biology* 16 (7): 2024–2038. https://doi.org/10.1111/j.1365-2486.2009.02156.x.
- Chen, Y., S. Hantson, N. Andela, S.R. Coffield, C.A. Graff, D.C. Morton, L.E. Ott, E. Foufoula-Georgiou, P. Smyth, M.L. Goulden, and J.T. Randerson. 2022. California wildfire spread derived using VIIRS satellite observations and an object-based tracking system. *Scientific Data* 9 (1): 249. https://doi.org/10.1038/s41597-022-01343-0.
- Coop, J.D., T.J. DeLory, W.M. Downing, S.L. Haire, M.A. Krawchuk, C. Miller, M.-A. Parisien, and R.B. Walker. 2019. Contributions of fire refugia to resilient ponderosa pine and dry mixed-conifer forest landscapes. *Ecosphere* 10 (7): e02809. https://doi.org/10.1002/ecs2.2809.
- Crutzen, P.J., and M.O. Andreae. 1990. Biomass burning in the tropics: Impact on atmospheric chemistry and biogeochemical cycles. *Science* 250 (4988): 1669–1678. https://doi.org/10.1126/science.250.4988.1669.
- Cunningham, C.X., G.J. Williamson, and D.M.J.S. Bowman. 2024. Increasing frequency and intensity of the most extreme wildfires on earth. *Nature Ecology & Evolution* 8 (8): 1420–1425. https://doi.org/10.1038/s41559-024-02452-2.
- De Luis, M., M.J. Baeza, J. Raventós, and J.C. González-Hidalgo. 2004. Fuel characteristics and fire behaviour in mature Mediterranean gorse shrublands. *International Journal of Wildland Fire* 13 (1): 79. https://doi.org/10.1071/WF03005.
- Debano, L.F. 2000. The role of fire and soil heating on water repellency in wildland environments: A review. *Journal of Hydrology*. https://doi.org/10.1016/S0022-1694(00)00194-3.
- Dillon, G. K., Z. A. Holden, P. Morgan, M. A. Crimmins, E. K. Heyerdahl, and C. H. Luce. 2011. Both topography and climate affected forest and woodland burn severity in two regions of the western US, 1984 to 2006. *Ecosphere* 2 (12): 130. https://doi.org/10.1890/ES11-00271.1.
- Doerr, S. H., W. H. Blake, R. A. Shakesby, F. Stagnitti, S. H. Vuurens, G. S. Humphreys, P. Wallbrink, S. H. Doerr, W. H. Blake, R. A. Shakesby, F. Stagnitti, S. H. Vuurens, G. S. Humphreys, and P. Wallbrink. 2004. Heating effects on water repellency in Australian eucalypt forest soils and their value in estimating wildfire soil temperatures. *International Journal of Wildland Fire* 13 (2): 157–163. https://doi.org/10.1071/WF03051.
- Eidenshink, J., B. Schwind, K. Brewer, Z.-L. Zhu, B. Quayle, and S. Howard. 2007. A project for monitoring trends in burn severity. *Fire Ecology* 3 (1): 3–21. https://doi.org/10.4996/fireecology.0301003.
- Epting, J., D. Verbyla, and B. Sorbel. 2005. Evaluation of remotely sensed indices for assessing burn severity in interior Alaska using Landsat TM and ETM+. Remote Sensing of Environment 96 (3–4): 328–339. https://doi.org/10.1016/j.rse.2005.03.002.
- Estes, B.L., E.E. Knapp, C.N. Skinner, J.D. Miller, and H.K. Preisler. 2017. Factors influencing fire severity under moderate burning conditions in the Klamath Mountains, northern California, USA. *Ecosphere* 8 (5): e01794. https://doi.org/10.1002/ecs2.1794.
- Fernández-Guisuraga, J.M., S. Suárez-Seoane, P. García-Llamas, and L. Calvo. 2021. Vegetation structure parameters determine high burn severity likelihood in different ecosystem types: A case study in a burned Mediterranean landscape. *Journal of Environmental Management*. https://doi.org/10.1016/j.jenvman.2021.112462.
- Finney, M. 2006. An Overview of FlamMap Fire Modeling Capabilities (pp. 213–220). U.S. Department of Agriculture, Forest Service, Rocky Mountain Research Station. https://www.fs.usda.gov/research/treesearch/25948
- Finney, M. A., C. W. McHugh, I. C. Grenfell, K. L. Riley, and K. C. Short. 2011. A simulation of probabilistic wildfire risk components for the continental United States. *Stochastic Environmental Research and Risk Assessment* 25 (7): 973–1000. https://doi.org/10.1007/s00477-011-0462-z.

- Florsheim, J. L., E. A. Keller, and D. W. Best. 1991. Fluvial sediment transport in response to moderate storm flows following chaparral wildfire, Ventura County, southern California. *Geological Society of America Bulletin*. https://doi.org/10.1130/0016-7606(1991)103%3c0504;FSTIRT%3e2.3.CO;2.
- Florsheim, J. L., A. Chin, L. S. O'Hirok, and R. Storesund. 2016. Short-term post-wildfire dry-ravel processes in a chaparral fluvial system. *Geomorphology*. https://doi.org/10.1016/j.geomorph.2015.03.035.
- The National Strategy: The Final Phase in the Development of the National Cohesive Wildland Fire Management Strategy. 2014. U.S. Forest and Rangelands.
- Gabet, E.J. 2003. Sediment transport by dry ravel. *Journal of Geophysical Research: Solid Earth*. https://doi.org/10.1029/2001jb001686.
- Giglio, L. 2007. Characterization of the tropical diurnal fire cycle using VIRS and MODIS observations. *Remote Sensing of Environment* 108 (4): 407–421. https://doi.org/10.1016/j.rse.2006.11.018.
- Giglio, L. 2018. MODIS collection 4 active fire product user's guide table of contents. *Revisión B. Nasa* 1 (June): 64.
- Giglio, L., W. Schroeder, and C.O. Justice. 2016. The collection 6 MODIS active fire detection algorithm and fire products. *Remote Sensing of Environment* 178: 31–41. https://doi.org/10.1016/j.rse.2016.02.054.
- Hantson, S., S. Pueyo, and E. Chuvieco. 2015. Global fire size distribution is driven by human impact and climate. *Global Ecology and Biogeography* 24 (1): 77–86. https://doi.org/10.1111/geb.12246.
- Hantson, S., N. Andela, M. L. Goulden, and J. T. Randerson. 2022. Humanignited fires result in more extreme fire behavior and ecosystem impacts. *Nature Communications*. https://doi.org/10.1038/s41467-022-30030-2.
- Hao, W. M., and M.-H. Liu. 1994. Spatial and temporal distribution of tropical biomass burning. Global Biogeochemical Cycles 8 (4): 495–503. https:// doi.org/10.1029/94GB02086.
- He, K., X. Shen, C. Merow, E. Nikolopoulos, R. V. Gallagher, F. Yang, and E. N. Anagnostou. 2024. Improving fire severity prediction in south-eastern Australia using vegetation-specific information. *Natural Hazards and Earth System Sciences* 24 (10): 3337–3355. https://doi.org/10.5194/ nhess-24-3337-2024.
- Heward, H., A.M.S. Smith, D.P. Roy, W.T. Tinkham, C.M. Hoffman, P. Morgan, and K.O. Lannom. 2013. Is burn severity related to fire intensity? Observations from landscape scale remote sensing. *International Journal of Wildland Fire* 22 (7): 910–918. https://doi.org/10.1071/WF12087.
- Holden, Z.A., P. Morgan, and J.S. Evans. 2009. A predictive model of burn severity based on 20-year satellite-inferred burn severity data in a large southwestern US wilderness area. *Forest Ecology and Management* 258 (11): 2399–2406. https://doi.org/10.1016/j.foreco.2009.08.017.
- Johnston, J.M., N. Jackson, C. McFayden, L. Ngo Phong, B. Lawrence, D. Davignon, M.J. Wooster, H. Van Mierlo, D.K. Thompson, A.S. Cantin, D. Johnston, L.M. Johnston, M. Sloane, R. Ramos, and T.J. Lynham. 2020. Development of the user requirements for the Canadian WildFireSat satellite mission. Sensors 20 (18): 5081. https://doi.org/10.3390/s20185081.
- Kang, S., J.S. Kimball, and S.W. Running. 2006. Simulating effects of fire disturbance and climate change on boreal forest productivity and evapotranspiration. Science of the Total Environment 362 (1–3): 85–102. https://doi.org/10.1016/j.scitotenv.2005.11.014.
- Kasischke, E.S., N.L. Christensen Jr., and B.J. Stocks. 1995. Fire, global warming, and the carbon balance of boreal forests. *Ecological Applications* 5 (2): 437–451. https://doi.org/10.2307/1942034.
- Kean, J.W., D.M. Staley, and S.H. Cannon. 2011. In situ measurements of post-fire debris flows in southern California: Comparisons of the timing and magnitude of 24 debris-flow events with rainfall and soil moisture conditions. *Journal of Geophysical Research* 116 (F4): F04019. https://doi.org/10.1029/2011JF002005.
- Keeley, J.E., C.J. Fotheringham, and M. Morais. 1999. Reexamining fire suppression impacts on brushland fire regimes. *Science* 284 (5421): 1829–1832. https://doi.org/10.1126/science.284.5421.1829.
- Key, C.H., and Benson, N.C. 2006. Landscape Assessment (LA) sampling and analysis methods. USDA Forest Service - General Technical Report RMRS-GTR.
- Lamb, M. P., J. S. Scheingross, W. H. Amidon, E. Swanson, and A. Limaye. 2011. A model for fire-induced sediment yield by dry ravel in steep landscapes. *Journal of Geophysical Research*. https://doi.org/10.1029/2010JF001878.
- Lamb, M. P., M. Levina, R. A. Dibiase, and B. M. Fuller. 2013. Sediment storage by vegetation in steep bedrock landscapes: Theory, experiments, and implications for postfire sediment yield. *Journal of Geophysical Research-Earth Surface*. https://doi.org/10.1002/jgrf.20058.

- Lancaster, J.T., B.J. Swanson, S.G. Lukashov, N.S. Oakley, J.B. Lee, E.R. Spangler, J.L. Hernandez, B.P.E. Olson, M.J. Defrisco, D.N. Lindsay, Y.J. Schwartz, S.E. Mccrea, P.D. Roffers, and C.M. Tran. 2021. Observations and analyses of the 9 January 2018 debris-flow disaster, Santa Barbara County, California. *Environmental and Engineering Geoscience*, no. 1. https://doi.org/10.2113/EEG-D-20-00015.
- Letey, J. 2001. Causes and consequences of fire-induced soil water repellency. *Hydrological Processes*. https://doi.org/10.1002/hyp.378.
- Li, F., X. Zhang, S. Kondragunta, and D. P. Roy. 2018. Investigation of the fire radiative energy biomass combustion coefficient: A comparison of polar and geostationary satellite retrievals over the conterminous United States. *Journal of Geophysical Research: Biogeosciences* 123 (2): 722–739. https://doi.org/10.1002/2017JG004279.
- Li, F., X. Zhang, S. Kondragunta, X. Lu, I. Csiszar, and C. C. Schmidt. 2022. Hourly biomass burning emissions product from blended geostationary and polar-orbiting satellites for air quality forecasting applications. *Remote Sensing of Environment* 281: 113237. https://doi.org/10.1016/j.rse.2022.
- Linn, R., J. Reisner, J. J. Colman, and J. Winterkamp. 2002. Studying wildfire behavior using FIRETEC. *International Journal of Wildland Fire* 11 (4): 233. https://doi.org/10.1071/WF02007.
- Linn, R. R., S. L. Goodrick, S. Brambilla, M. J. Brown, R. S. Middleton, J. J. O'Brien, and J. K. Hiers. 2020. QUIC-fire: A fast-running simulation tool for prescribed fire planning. *Environmental Modelling & Software* 125: 104616. https://doi.org/10.1016/j.envsoft.2019.104616.
- Liu, T., J.T. Randerson, Y. Chen, D.C. Morton, E.B. Wiggins, P. Smyth, E. Foufoula-Georgiou, R. Nadler, and O. Nevo. 2024. Systematically tracking the hourly progression of large wildfires using GOES satellite observations. *Earth System Science Data* 16 (3): 1395–1424. https://doi.org/10.5194/essd-16-1395-2024.
- Lizundia-Loiola, J., G. Otón, R. Ramo, and E. Chuvieco. 2020. A spatio-temporal active-fire clustering approach for global burned area mapping at 250 m from MODIS data. *Remote Sensing of Environment* 236: 111493. https://doi.org/10.1016/j.rse.2019.111493.
- Loboda, T.V., and I.A. Csiszar. 2007. Reconstruction of fire spread within wild-land fire events in Northern Eurasia from the MODIS active fire product. *Global and Planetary Change* 56 (3–4): 258–273. https://doi.org/10. 1016/j.qloplacha.2006.07.015.
- Luo, K., X. Wang, M. De Jong, and M. Flannigan. 2024. Drought triggers and sustains overnight fires in North America. *Nature* 627 (8003): 321–327. https://doi.org/10.1038/s41586-024-07028-5.
- Mell, W., M. A. Jenkins, J. Gould, and P. Cheney. 2007. A physics-based approach to modelling grassland fires. *International Journal of Wildland Fire* 16 (1): 1. https://doi.org/10.1071/WF06002.
- Miller, J.D., and A.E. Thode. 2007. Quantifying burn severity in a heterogeneous landscape with a relative version of the delta normalized burn ratio (dNBR). Remote Sensing of Environment 109 (1): 66–80. https://doi.org/10.1016/j.rse.2006.12.006.
- Morgan, P., R. E. Keane, G. K. Dillon, T. B. Jain, A. T. Hudak, E. C. Karau, P. G. Sikkink, Z. A. Holden, and E. K. Strand. 2014. Challenges of assessing fire and burn severity using field measures, remote sensing and modelling. International Journal of Wildland Fire 23 (8): 1045. https://doi.org/10.1071/WF13058.
- Mu, M., J. T. Randerson, G. R. Van Der Werf, L. Giglio, P. Kasibhatla, D. Morton, G. J. Collatz, R. S. DeFries, E. J. Hyer, E. M. Prins, D. W. T. Griffith, D. Wunch, G. C. Toon, V. Sherlock, and P. O. Wennberg. 2011. Daily and 3-hourly variability in global fire emissions and consequences for atmospheric model predictions of carbon monoxide: Daily and hourly global fire emissions. *Journal of Geophysical Research: Atmospheres* 116 (D24): n/a-n/a. https://doi.org/10.1029/2011JD016245.
- Mueller, S.E., A.E. Thode, E.Q. Margolis, L.L. Yocom, J.D. Young, and J.M. Iniguez. 2020. Climate relationships with increasing wildfire in the southwestern US from 1984 to 2015. Forest Ecology and Management. https://doi.org/10.1016/j.foreco.2019.117861.
- Neff, J. C., J. W. Harden, and G. Gleixner. 2005. Fire effects on soil organic matter content, composition, and nutrients in boreal interior Alaska. *Canadian Journal of Forest Research* 35 (9): 2178–2187. https://doi.org/10.1139/x05-154.
- O'Connor, C. D., D. E. Calkin, and M. P. Thompson. 2017. An empirical machine learning method for predicting potential fire control locations for pre-fire planning and operational fire management. *International Journal of Wildland Fire* 26 (7): 587. https://doi.org/10.1071/wf16135.

Orland et al. Fire Ecology (2025) 21:55 Page 18 of 18

- Olson, D. M., E. Dinerstein, E. D. Wikramanayake, N. D. Burgess, G. V. N. Powell, E. C. Underwood, J. A. D'amico, I. Itoua, H. E. Strand, J. C. Morrison, C. J. Loucks, T. F. Allnutt, T. H. Ricketts, Y. Kura, J. F. Lamoreux, W. W. Wettengel, P. Hedao, and K. R. Kassem. 2001. Terrestrial ecoregions of the world: A new map of life on Earth. *BioScience* 51 (11): 933. https://doi.org/10.1641/0006-3568(2001)051[0933:TEOTWA]2.0.CO;2.
- Parks, S., G. Dillon, and C. Miller. 2014. A new metric for quantifying burn severity: The relativized burn ratio. *Remote Sensing* 6 (3): 1827–1844. https://doi.org/10.3390/rs6031827.
- Picotte, JJ., and K.M. Robertson. 2011. Validation of remote sensing of burn severity in south-eastern US ecosystems. *International Journal of Wildland Fire* 20 (3): 453. https://doi.org/10.1071/WF10013.
- Ponomarev, E.I., A.N. Zabrodin, E.G. Shvetsov, and T.V. Ponomareva. 2023. Wildfire intensity and fire emissions in Siberia. *Fire* 6 (7): 246. https://doi.org/10. 3390/fire6070246.
- Randerson, J. T., H. Liu, M. G. Flanner, S. D. Chambers, Y. Jin, P. G. Hess, G. Pfister, M. C. Mack, K. K. Treseder, L. R. Welp, F. S. Chapin, J. W. Harden, M. L. Goulden, E. Lyons, J. C. Neff, E. A. G. Schuur, and C. S. Zender. 2006. The impact of boreal forest fire on climate warming. *Science* 314 (5802): 1130–1132. https://doi.org/10.1126/science.1132075.
- Robichaud, P.R., and R.D. Hungerford. 2000. Water repellency by laboratory burning of four northern Rocky Mountain forest soils. *Journal of Hydrology* 231: 207–219. https://doi.org/10.1016/S0022-1694(00)00195-5.
- Roche, J.W., M.L. Goulden, and R.C. Bales. 2018. Estimating evapotranspiration change due to forest treatment and fire at the basin scale in the Sierra Nevada, California. *Ecohydrology* 11 (7): e1978. https://doi.org/10.1002/ecc1978
- Rollins, M.G. 2009. LANDFIRE: A nationally consistent vegetation, wildland fire, and fuel assessment. *International Journal of Wildland Fire* 18 (3): 235. https://doi.org/10.1071/WF08088.
- Rothermel, R. 1972. A mathematical model for predicting fire spread in wildland fuels. https://research.fs.usda.gov/treesearch/32533
- Rovira, P., J. Romanyà, and B. Duguy. 2012. Long-term effects of wildfires on the biochemical quality of soil organic matter: A study on Mediterranean shrublands. *Geoderma* 179:9–19. https://doi.org/10.1016/j.geoderma. 2012.02.011.
- Scaduto, E., B. Chen, and Y. Jin. 2020. Satellite-based fire progression mapping: A comprehensive assessment for large fires in northern California. *IEEE Journal of Selected Topics in Applied Earth Observations and Remote Sensing* 13: 5102–5114. https://doi.org/10.1109/JSTARS.2020.3019261.
- Schroeder, W., and Giglio, L. 2016. Visible Infrared Imaging Radiometer Suite (VIIRS) 375 m Active Fire Detection and Characterization Algorithm Theoretical Basis Document 1.0.
- Schroeder, W., P. Oliva, L. Giglio, and I. A. Csiszar. 2014. The new VIIRS 375 m active fire detection data product: Algorithm description and initial assessment. *Remote Sensing of Environment* 143:85–96. https://doi.org/10.1016/j.rse. 2013.12.008.
- Schwilk, D. W., and D. D. Ackerly. 2001. Flammability and serotiny as strategies: Correlated evolution in pines. *Oikos* 94 (2): 326–336. https://doi.org/10.1034/j.1600-0706.2001.940213.x.
- Scott, J.H., and Burgan, R.E. 2005. Standard fire behavior fuel models: A comprehensive set for use with Rothermel's surface fire spread model. U.S. Department of Agriculture, Forest Service, Rocky Mountain Research Station. https://doi.org/10.2737/rmrs-gtr-153
- Scott, D.F., D.B. Versfeld, and W. Lesch. 1998. Erosion and sediment yield in relation to afforestation and fire in the mountains of the Western Cape Province, South Africa. South African Geographical Journal 80 (1): 52–59. https://doi. org/10.1080/03736245.1998.9713644.
- Seiler, W., and P. J. Crutzen. 1980. Estimates of gross and net fluxes of carbon between the biosphere and the atmosphere from biomass burning. Climatic Change 2 (3): 207–247. https://doi.org/10.1007/BF00137988.
- Seydi, S.T., J.T. Abatzoglou, A. AghaKouchak, Y. Pourmohamad, A. Mishra, and M. Sadegh. 2024. Predictive understanding of links between vegetation and soil burn severities using physics-informed machine learning. *Earth's Future* 12 (8): e2024EF004873. https://doi.org/10.1029/2024EF004873.
- Staley, D. M., A. C. Tillery, J. W. Kean, L. A. McGuire, H. E. Pauling, F. K. Rengers, and J. B. Smith. 2018. Estimating post-fire debris-flow hazards prior to wildfire using a statistical analysis of historical distributions of fire severity from remote sensing data. *International Journal of Wildland Fire* 27 (9): 595. https://doi.org/10.1071/WF17122.

- Thompson, M.P., C.D. O'Connor, B.M. Gannon, M.D. Caggiano, C.J. Dunn, C.A. Schultz, D.E. Calkin, B. Pietruszka, S.M. Greiner, R. Stratton, and J.T. Morisette. 2022. Potential operational delineations: New horizons for proactive, risk-informed strategic land and fire management. *Fire Ecology* 18 (1): 17. https://doi.org/10.1186/s42408-022-00139-2.
- Wildfire Crisis Implementation Plan. 2022. U.S. Forest Service. https://www.fs.usda. gov/sites/default/files/Wildfire-Crisis-Implementation-Plan.pdf
- Van Der Werf, G.R., J.T. Randerson, G.J. Collatz, and L. Giglio. 2003. Carbon emissions from fires in tropical and subtropical ecosystems. *Global Change Biology* 9 (4): 547–562. https://doi.org/10.1046/j.1365-2486.2003.00604.x.
- Van Der Werf, G. R., J. T. Randerson, L. Giglio, T. T. Van Leeuwen, Y. Chen, B. M. Rogers, M. Mu, M. J. E. Van Marle, D. C. Morton, G. J. Collatz, R. J. Yokelson, and P. S. Kasibhatla. 2017. Global fire emissions estimates during 1997–2016. *Earth System Science Data* 9 (2): 697–720. https://doi.org/10.5194/essd-9-697-2017.
- Vega, J.A., and F. Díaz-Fierros Viqueira. 1987. Wild fire effects on soil erosion. Ecologia Mediterranea 13 (4): 119–125. https://doi.org/10.3406/ecmed. 1987.1195.
- Veraverbeke, S., E.N. Stavros, and S.J. Hook. 2014. Assessing fire severity using imaging spectroscopy data from the Airborne Visible/Infrared Imaging Spectrometer (AVIRIS) and comparison with multispectral capabilities. Remote Sensing of Environment 154: 153–163. https://doi.org/10.1016/j.rse. 2014.08.019.
- Wells, W.G. 1981. Some effects of brushfires on erosion processes in coastal southern California. *Erosion and Sediment Transport in Pacific Rim Steeplands. Proc. Christchurch Symposium, January 1981*.
- Wells, A. G., T. J. Hawbaker, J. K. Hiers, J. Kean, R. A. Loehman, and P. F. Steblein. 2023. Predicting burn severity for integration with post-fire debris-flow hazard assessment: A case study from the Upper Colorado River Basin, USA. International Journal of Wildland Fire 32 (9): 1315–1331. https://doi. org/10.1071/wf22200.
- Westerling, A.L., H.G. Hidalgo, D.R. Cayan, and T.W. Swetnam. 2006. Warming and earlier spring increase Western U.S. forest wildfire activity. *Science*. https://doi.org/10.1126/science.1128834.
- Whitman, E., M. Parisien, D. K. Thompson, R. J. Hall, R. S. Skakun, and M. D. Flannigan. 2018. Variability and drivers of burn severity in the northwestern Canadian boreal forest. *Ecosphere* 9 (2): e02128. https://doi.org/10.1002/ecs2.2128.
- Wiggins, E. B., A. J. Soja, E. Gargulinski, H. S. Halliday, R. B. Pierce, C. C. Schmidt, J. B. Nowak, J. P. DiGangi, G. S. Diskin, J. M. Katich, A. E. Perring, J. P. Schwarz, B. E. Anderson, G. Chen, E. C. Crosbie, C. Jordan, C. E. Robinson, K. J. Sanchez, T. J. Shingler, Michael Shook, Kenneth L.. Thornhill, Edward L.. Winstead, Luke D.. Ziemba, and R. H. Moore. 2020. High temporal resolution satellite observations of fire radiative power reveal link between fire behavior and aerosol and gas emissions. Geophysical Research Letters. https://doi.org/10.1079/7020G1.090707.
- Wooster, M. J., G. Roberts, G. L. W. Perry, and Y. J. Kaufman. 2005. Retrieval of biomass combustion rates and totals from fire radiative power observations: FRP derivation and calibration relationships between biomass consumption and fire radiative energy release. *Journal of Geophysical Research* 110 (D24): D24311. https://doi.org/10.1029/2005JD006318.
- Wu, Z., H. S. He, Y. Liang, L. Cai, and B. J. Lewis. 2013. Determining relative contributions of vegetation and topography to burn severity from Landsat imagery. *Environmental Management* 52 (4): 821–836. https://doi.org/10.1007/s00267-013-0128-3.
- Young, J. D., E. Belval, B. Gannon, Y. Wei, C. O'Connor, C. Dunn, B. M. Pietruszka, D. Calkin, and M. Thompson. 2024. The cost of operational complexity: A causal assessment of pre-fire mitigation and wildfire suppression. Forest Policy and Economics 169: 103351. https://doi.org/10.1016/j.forpol.2024. 103351

Publisher's Note

Springer Nature remains neutral with regard to jurisdictional claims in published maps and institutional affiliations.